Magnetoelectric properties of the Co/PbZr$_x$Ti$_{1-x}$O$_3$ (001) interface studied from first principles

V. S. Borisov,[1,*] S. Ostanin,[1] I. V. Maznichenko,[2] A. Ernst,[1] and I. Mertig[1,2]
[1]*Max Planck Institute of Microstructure Physics, Weinberg 2, D-06120 Halle, Germany*
[2]*Institute of Physics, Martin Luther University Halle-Wittenberg, D-06099 Halle, Germany*
(Received 7 November 2013; revised manuscript received 14 February 2014; published 28 February 2014)

Magnetoelectric coupling at the interface between PbTi(Zr)O$_3$ (001) (PZT) and a Co film as well as its tuning by Zr substitutions is studied here from first principles. Chemically disordered 25% Zr-doped compositions were modeled within the supercell approach. Our calculations suggest that ferroelectric ionic displacements in PZT can be locally enhanced, especially when the interfacial Ti cations are replaced with Zr. Regarding Co films their structure tends to become hexagonal for thicker films, while rather significant changes in Co magnetization are anticipated in response to the electric polarization reversal in PZT.

DOI: 10.1103/PhysRevB.89.054436 PACS number(s): 75.85.+t, 75.47.Lx

I. INTRODUCTION

Multiferroic tunnel junctions, with ferroelectric barriers, have motivated research in the last decade due to their capability of tuning spin transport by an external electric field [1–7]. Here, the polarization reversal of the tunneling barrier changes the interface magnetoelectricity and, as a result, affects the transport properties of multiferroic tunnel junctions, thereby fabricating a so-called four-state memory device. Recently, Pantel *et al.* [8] demonstrated that the sign of the tunneling magnetoresistance (TMR) effect measured in La(Sr)MnO$_3$ (LSMO)/PbZr$_{0.2}$Ti$_{0.8}$O$_3$ (001) (PZT)/Co can be robustly switched by the polarization reversal of PZT. The observation is attributed mostly to a strong magnetoelectric coupling (MEC) at the Co/PZT interface, whereas the other interface, between LSMO and PZT, as the authors suggested [8], may not contribute very much to the effect. Recent findings [9,10] support this hypothesis for the chosen composition, $x = 0.33$, of LSMO.

Theoretical studies of the Co/PZT interface from first principles have not been reported so far. It would be worthwhile to investigate the role of the Zr impurities in PZT on interfacial MEC. In our *ab initio*–based work, we compute both the [001]-oriented Co/PZT and the Co/PTO (PbTiO$_3$) interfaces, focusing on the electronic mechanism of the interfacial MEC, while Zr doping is modeled within the supercell approach.

The paper is organized as follows: In Sec. II we describe the structural model and give the details of our calculations. In Sec. III, important issues concerning the influence of Zr doping on the structural features and the interface bonding are addressed. The electronic mechanism of the observed MEC effect is outlined in Sec. IV for both undoped and Zr-doped interfaces. The electronic origin of this effect and its role in the spin-dependent transport properties of the corresponding tunnel junctions is the subject of Sec. V. Finally, we summarize the results of our *ab initio* study and discuss further research venues in Sec. VI.

II. DETAILS OF CALCULATIONS

A. Co/PTO

All calculations were performed using the Vienna *Ab Initio* Simulation Package (VASP) [11–13], within the generalized gradient approximation (GGA-PBE) [14] to the exchange-correlation potential. Electron-ion interactions were described by projector-augmented wave pseudopotentials [15], and electronic wave functions were represented by plane waves with a cutoff energy of 460 eV. Ionic relaxation of the interfaces was performed using the Γ-centered k-point Monkhorst-Pack [16] mesh and the conjugate gradient algorithm until the Hellmann-Feynman forces became less than 5×10^{-3} eV/Å. For undoped Co/PTO supercells the use of a $6 \times 6 \times 3$ **k** mesh yields reliable results. Density of states (DOS) calculations were performed using the tetrahedron method on the same **k** mesh.

Experimentally, the SrTiO$_3$ (001) (STO) substrate was used to grow LSMO/PZT/Co [8]. Since the in-plane STO lattice parameter (3.898 Å) is very close to that of bulk PTO (3.892 Å), we fixed $a = 3.892$ Å for all supercells, keeping $c/a = 1.071$ within the ferroelectric side before relaxation. This setup may simulate epitaxial growth on the STO substrate, as performed in Ref. [8]. Thus, the starting intralayer displacements between the cations and the anions of PTO were optimized as 0.45 and 0.33 Å for the PbO and TiO$_2$ layers, respectively. This is in reasonable agreement with experiment. We simulated the Co/PTO (001) interface with supercells which contain five unit cells of PTO stacked along [001] and different numbers, n, of cobalt layers, as shown in Fig. 1. The vacuum of about 15 Å added above the Co layers is sufficiently large to eliminate any interactions between the periodic images of the supercell along the [001] axis. We varied the Co thickness between $n = 5$ and $n = 7$. Additionally, the effect of Au capping was simulated by adding two Au layers above the Co$_{n=5}$ structure, which allows us to exclude the effect from the ferromagnetic Co surface.

The atomic positions of the three PTO u.c. starting from the third one next to the interface were fixed during the relaxation to conserve the chosen electric polarization state, whereas all atoms of the 2 PTO u.c. near the interface were allowed to relax. To mimic the polarization reversal we used the procedure described in Ref. [17]. That allows us to compute

*vborisov@mpi-halle.mpg.de

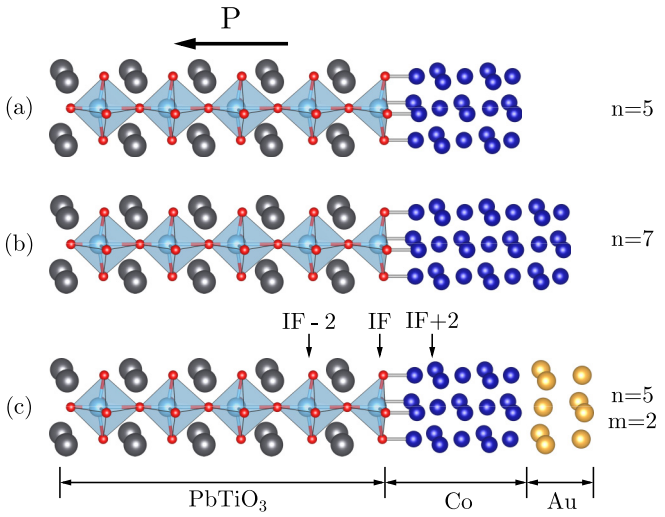

FIG. 1. (Color online) Side view of the (a, b) $(Co_2)_n/(PbTiO_3)_5$ (001) and (c) $(Au_2)_m/(Co_2)_n/(PbTiO_3)_5$ (001) supercells, where n and m denote the number of cobalt and gold layers, respectively. Each Co/Au layer contains two atoms per unit cell surface area of PTO. The interfacial TiO_2 layer, which terminates PTO, is labeled IF, whereas the Co layers outward from the interface are labeled IF+1, IF+2, and so on. The polarization direction of PTO, namely, $P_\downarrow$, is shown by the arrow.

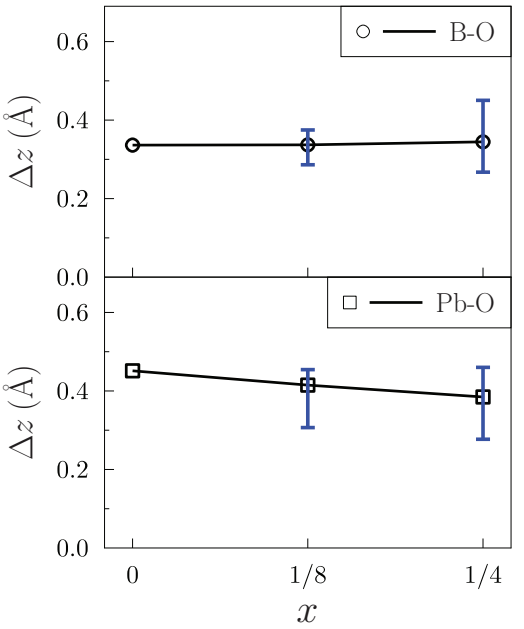

FIG. 2. (Color online) Relaxed ionic displacements Δz in Pb $Zr_xTi_{1-x}O_3$ calculated for $x = 0$, $1/8$, and $1/4$. The solid line corresponds to the Δz average. The variation range of Δz in the supercell is marked by vertical bars.

and compare the two cases of polarization in PTO: $P_\downarrow$ and $P_\uparrow$, where the cations and anions of each atomic layer were displaced along [001] in accordance with the polarization state. For the polarization state $P_\downarrow$, for instance, all oxygens are placed above the cations in each monolayer, as shown in Fig. 1, and vice versa. Regarding the Co side, we optimized all metal atoms. After that one can compare the structural changes near the interface for each polarization state. As a result, the variation of the electronic states and magnetic properties of Co/PTO upon polarization reversal is discussed.

The crystal structure of the Co film needs special attention. Each interfacial Co atom is situated above the oxygen ion, which belongs to the TiO_2 termination of PTO, as Pantel *et al.* [8] suggested. Surface x-ray diffraction studies of thin $BaTiO_3$ (BTO) films [18,19] grown on Fe (001) also show that the interface bonding is mediated between the O atoms atop the Fe atoms. These experimental findings confirm all previous *ab initio* studies for the energetically favorable termination of Fe/BTO [17,20–22], Co/STO [23], and Co/BTO [24]. For thin Co films on PTO (001), the atomic arrangements of Co formally mimic a face-centered tetragonally distorted structure, with an in-plane lattice parameter of 3.892 Å, which corresponds to an in-plane Co-Co distance of 2.75 Å. In bulk hcp Co, the nearest Co atoms are separated by 2.51 Å, and therefore, the epitaxial Co film is subject to an in-plane tensile strain of about 9.6%.

Additionally, we analyzed the structural features of cobalt using statically relaxed supercells and *ab initio* molecular dynamics simulations implemented in VASP. For molecular dynamics simulations, Γ-point Brillouin-zone sampling was used. The time step was 1 fs. To obtain adequate statistics for thermodynamic equilibrium, we ran the simulations for a duration of 1.5 ps at a finite temperature equal to 1 K. All metal atoms were allowed to move. The first 0.1-ps outputs were excluded from the statistics.

B. Co/PZT

Before studying the interface of Co/PZT (001) we simulated the Zr-doped bulk Pb $Zr_xTi_{1-x}O_3$ (PZT) within the supercell approach. The structure and ferroelectricity of bulk PZT critically depend on the Zr/Ti composition. Below the concentration $x < 0.52$, it adopts a tetragonally distorted perovskite structure, with spontaneous polarization of 50–60 $\mu C/cm^2$ oriented along [001] [25]. In our calculations, we modeled the compositions $x = 1/8$ and $x = 1/4$ using a $2 \times 2 \times 2$ perovskite supercell, which contains eight unit cells of PTO. The experimental lattice parameters were used. For $x = 1/8$, we replaced one of the Ti cations with Zr and completely relaxed the positions of atoms. For $x = 1/4$, there are five options to distribute two Zr across the eight B sites. Each case was inspected after relaxation. The ferroelectric displacements, Δz, are important in this context, while the presence of Zr changes them locally. In particular, for a single Zr impurity in the supercell the relaxed Δz is enhanced for the nearest Ti cations, whereas it becomes slightly diminished for the next-nearest Pb cations. In general, Zr doping leads to variations of Δz across the supercell. The larger x, the more strongly the Δz vary, as shown in Fig. 2. For the two Zr dopants ($x = 1/4$), after configurational averaging we found that the Δz were not changed significantly for B cations, while the corresponding Δz were moderately decreased for A cations.

The Co/PZT (001) interface was simulated with two models. The first model corresponds to a digital Zr-O monolayer, whose position near the interface was varied using the supercell shown in Fig. 1(c). When ZrO_2 terminates

PTO (001), it corresponds to the composition $2 \times Au_2/5 \times Co_2/ZrO_2/PbO/TiO_2/PbO/TiO_2/PbO/\ldots$. We also replaced the third PTO layer from the interface with a ZrO_2 monolayer. Obviously, the Zr dopant forms, in this case, an atomic layer of ZrO_2 perpendicular to the growth direction.

For the second model of Co/PZT (001) we started from a $2 \times 2 \times 2$ bulk perovskite supercell. It contains four unit cells of perovskite in the x-y plane and allows us to simulate the $Zr_{0.25}Ti_{0.75}O_2$ composition in the topmost BO_2 layer of PZT that is put in contact with the cobalt film. This effective doping can be achieved by replacing randomly one of every four titanium cations with a Zr impurity. Thus, we can mimic the effect of substitutional disorder on the ferroic and structural properties of Co/PZT (001). The topmost one-unit-cell-thick PZT side and all seven metal layers, each consisting of eight atoms, were relaxed.

III. STRUCTURE

A. Ferroelectric substrate

As the first step, we studied the structure of the Co/PZT interface after relaxation in comparison with that of Co/PTO. The intralayer ionic displacements in the PbO and Ti(Zr)O_2 layers along [001] can characterize the local ferroelectric properties. We found that near the Co/PTO interface in polarization state $P_\downarrow$, i.e., for $\vec{P}$ pointing away from the Co film, the cation-oxygen displacements after relaxation were increased (especially for the second PbO layer, IF-1) compared to the bulk displacements. This is shown in the lower left panel in Fig. 3. However, the same system in polarization state $P_\uparrow$ shows a noticeable local suppression of ferroelectric displacements for the interfacial TiO_2 layer, IF, as shown in the upper left panel in Fig. 3. It should be noted that state $P_\downarrow$ is energetically favorable by 1.2 eV per supercell, which is shown in Fig. 1(c). The energy imbalance between the two polarizations is qualitatively similar to the case of the TiO_2-terminated free PTO (001) surface discussed in

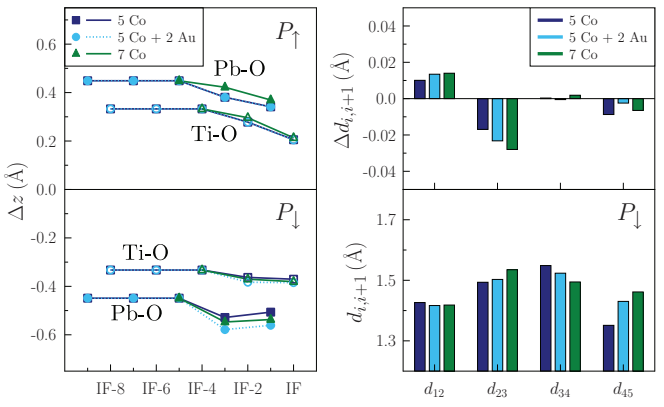

FIG. 3. (Color online) Intralayer cation-anion displacements along [001], Δz(Pb-O) and Δz(Ti-O), calculated for the PTO side of the interface, are shown in the left panel for the electric polarization directions $P_\uparrow$ and $P_\downarrow$. Interlayer distances in the Co film for the $P_\downarrow$ state and its variations $\Delta d_{i,i+1}$ upon polarization reversal are plotted in the right panel for varied numbers of cobalt monolayers. The case of the two-monolayer-thick Au-capped Co/PTO is shown as well.

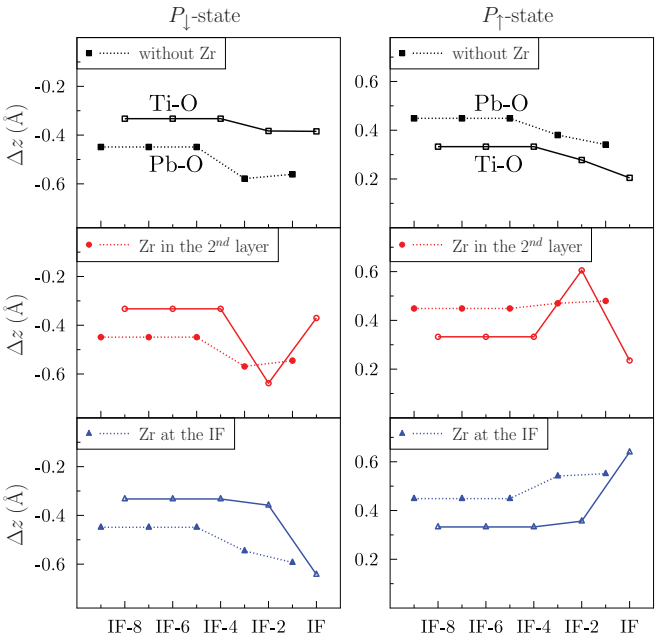

FIG. 4. (Color online) Intralayer displacements Δz(Pb-O) and Δz(Ti-O) on the ferroelectric Pb $Zr_{0.2}Ti_{0.8}O_3$ side calculated for two polarizations, $P_\downarrow$ (left panel) and $P_\uparrow$ (right panel). The two positions of the Zr impurity in PZT are shown in comparison with the pure Co/PTO interface.

Ref. [17]. The perovskite surface prefers an atomic arrangement with oxygens placed slightly above the larger cations to form a flat charge isosurface. Thus, for the Co/PTO interface we find its structure features rather different from those of the PTO (001) surface. Obviously, the interfacial Co-O bonds and related charge screening from the multiple cobalt layers introduce all structural changes, which are plotted in Fig. 3 and which, in general, were not expected from the ferroelectric surface consideration.

For the Co/PZT interface, with the structure of a digital alloy, i.e., when Zr replaces all Ti in layer IF or IF-2, relaxed displacements Δz were enhanced locally by factor of almost 2 at the sites occupied by Zr atoms even for an energetically unfavorable polarization state (Fig. 4). These results were supported by our calculations for the 2×2 in-plane supercell, which mimics a 25% Zr composition in each TiO_2 layer. In this case and for layer IF, the corresponding Δz increases locally by ~56%. Such behavior was expected from simulations of the bulk alloy Pb $Zr_xTi_{1-x}O_3$.

The electronic properties of multiferroics strongly depend on the interfacial bond lengths, which in our case are the interatomic distances between Co and oxygen. For pure Co/PTO, we found that the corresponding distance, d(Co-O), depends on $\vec{P}$ and increases from 1.90 to 1.98 Å upon switching, as reported in Table I. The variation of the Co-O bond length affects the orbital hybridization, thereby changing the interplay between ionic character and covalency. When the Zr impurity is placed at the interface the $\vec{P}$-dependent effect is enhanced. For the latter we observe, within the digital alloy model, a remarkable change in the Co-O distance upon the polarization reversal from 1.91 to 2.98 Å, that is, by more than

TABLE I. Interatomic distance d(Co-O) and energy difference $\Delta E = E(P_\uparrow) - E(P_\downarrow)$ of the Co/PTO and Co/PZT interfaces, calculated within the digital alloy model. For Co/PZT, the two Zr positions are labeled IF and IF-2, which correspond to the interface and third PZT layer, respectively.

		Co/PZT	
	Co/PTO	IF-2	IF
d(Co-O) (Å)			
$P_\downarrow$	1.897	1.890	1.913
$P_\uparrow$	1.980	2.003	2.981
ΔE (eV/unit cell)	1.21	1.30	2.08

1 Å. This remarkable structural effect of doping is directly related to the large ionic radius of the Zr cation compared to that of Ti. The inherent feature of Zr-based oxide, namely, large ionic displacements in the ZrO planes, together with the polarization reversal, brings the interface oxygen atoms away from the Co cations for the $P_\uparrow$ state. The interface bonding is mediated, therefore, only through the Co-Zr pairs. On the other hand, the Zr digital doping in the third perovskite layer, IF-2, changes the interfacial bond length insignificantly. This implies the localized character of the effect. The predicted structural features should play an important role for the fabricated composite multiferroics, where the Zr impurities are randomly distributed across the PZT interface.

Using the 2×2 in-plane supercell, we simulated also the 25% Zr concentration at the interface, which mimics the experimental composition [8]. After relaxation both interfaces, Co/PTO and Co/PZT, possess some degree of roughness, shown as variation of their Co-O distances in Fig. 5. Whereas the roughness of the Co/PTO interface varies within 5%–6%, the presence of 25% Zr leads to rather significant variations in the Co-O bond length of up to 40%–50% for the energetically less preferable $P_\uparrow$ state. We also analyzed the case of doping with larger Hf cations, which are isovalent to Zr and Ti. Surprisingly, the Co/PHT system, with its larger species at the interface, is much closer structurally to the Co/PTO system than to Co/PZT. In all three systems studied here with the use of extended supercells, the average Co-O bond length increases under polarization reversal. The result is consistent with that of the digital alloy model.

B. Co film

There is another important issue concerning the structure of the cobalt film. For all studied structures, we found that the distance between atomic planes of cobalt ($d_{i,i+1}$) shows some pronounced variations along the [001] direction. Near the interfaces the interlayer separation, d_{12}, between the first two Co monolayers is considerably less than the next interlayer separation, d_{23}. For the case of Co/PTO this is shown in the right panel in Fig. 3. For five Co monolayers ($n = 5$) we observe the effect of the free cobalt surface, which is seen as a remarkable contraction between the topmost atomic planes. The side effect from the surface on the interface region was significantly weakened or even completely removed in our calculations for $n = 7$ and for five Co monolayers capped by a Au bilayer.

For the 1×1 in-plane supercell with two cobalt atoms in each Co layer deposited on robust ferroelectrics, such as PZT, we anticipate some minor changes in $d_{i,i+1}$ which depend on both the $\vec{P}$ direction and the Zr(Hf) position beneath the interface. The more degrees of freedom the Co layers had in our model, the more deviations were obtained. For instance, the use of a 2×2 supercell can already result in the Co structural reconstruction. The relaxed Co layers not only are contracted along [001], as one would expect because of strain, but also show rather noticeable in-plane displacements. This leads to a structure which differs from the tetragonally distorted fcc arrangement (Fig. 1). To illustrate the differences between the structures we performed *ab initio* molecular dynamics simulations. As the molecular dynamics output, we computed the radial distribution function, which characterizes the average Co-Co distance between nearest neighbors (Fig. 6). The similarity of radial distribution functions seen in all simulations indicates that the same type of structure in the cobalt film was obtained. When we compare the main RDF peak with that of bulk hcp Co, we see that the average nearest-neighbor Co-Co distance in Co/PTO and Co/PZT nanostructures is close to the bulk value, 2.51 Å. One can conclude that the distorted hcp crystal structure is stabilized in the epitaxially grown few-nanometers-thick Co film. However,

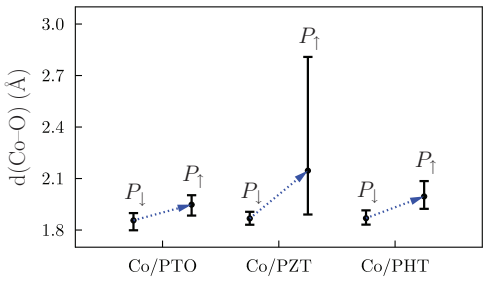

FIG. 5. (Color online) Co-O distances for Co/PTO and also for 25% Zr (Hf)–doped Co/PZT (Co/PHT) interfaces, modeled within the 2×2 in-plane supercell. Average values $\langle d \rangle$ are shown by filled circles and the spread of d is marked by vertical bars. Changes in $\langle d \rangle$ due to polarization reversal are additionally shown by dashed arrows.

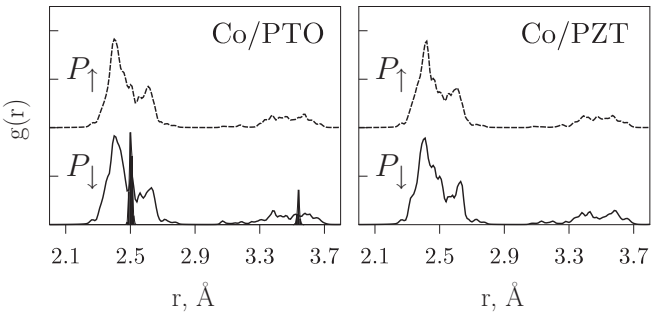

FIG. 6. Co-Co radial distribution functions calculated for the Co/PTO and 25%-doped Co/PZT interfaces in comparison with that of bulk hcp Co, which is represented by sharp shaded peaks in the left panel.

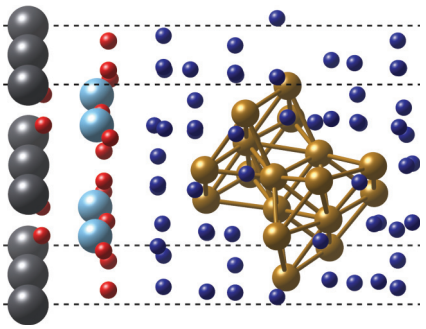

FIG. 7. (Color online) Formation of the Co hcp structural motif near the Co/PTO (001) interface for polarization $P_{\downarrow}$.

the c-axis direction differs from [001]. Indeed, for all studied interfaces, we found the characteristic hcp motif, which is inclined to the interface, as shown in Fig. 7 for the case of Co/PTO ($P_{\downarrow}$ state). The estimated lattice parameters a and c/a of this hcp unit cell are very close to the corresponding values for the bulk material, although the unit cell itself is moderately distorted with respect to the ideal structure. The "easy growing direction" for this hcp structure can be described by two angles: the polar angle θ measured relative to the [110] direction and the azimuthal angle φ determined relative to the [100] in-plane axis. The absolute values of the so-defined angles θ and φ are close to 45°. Within the fourfold in-plane C_{4v} symmetry of the metallic layer, the orientation of the hcp element and, generally, the structure of the cobalt film are not affected by Zr(Hf) doping or by the polarization reversal. It would be worthwhile to study the structure of thick cobalt films experimentally.

IV. MAGNETOELECTRIC EFFECT

By inspecting the distribution of the calculated magnetic moments in the Co film for the three cases of Co/PTO shown in Fig. 8, we can see that for the supercell with $n = 5$ there is a surface effect, which is significantly weakened when n is increased. For both polarization directions in PTO ($P_{\downarrow}$ and $P_{\uparrow}$), the Co film is strongly ferromagnetic.

For the Co/PTO interface, we anticipate a relatively strong MEC. There is a noticeable change in the magnetic moments in the interfacial Co layer IF+1 under polarization reversal (right panel in Fig. 8). On the other hand, as the system is switched to $P_{\uparrow}$, the induced magnetic moment of about 0.3 μ_B appears on the topmost Ti, while the small magnetic moments induced on interfacial oxygens became weaker due to the larger Co-O distance for the $P_{\uparrow}$ state (see Sec. III A). The overall spin polarization in the topmost TiO_2 layer is always opposite that of Co, although its magnitude is significantly higher for the $P_{\uparrow}$ state. Obviously, the MEC shows a localized character since it was observed in our calculations within the two atomic layers at the interface, namely, IF and IF+1, as shown in Fig. 1. The total magnetic moment, ΔM_{IF}, counted for the Co/PTO supercell as $Co_2{\cdot}TiO_2$, decreases by 0.65 μ_B upon polarization reversal. We attribute the observed MEC effect to the spin-dependent charge transfer from the Co film into the Ti d orbitals. Before, the same effect was discussed and illustrated for such multiferroics as Fe/BTO and Fe/PTO [20,26].

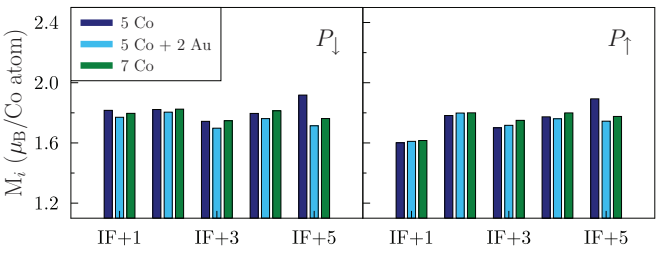

FIG. 8. (Color online) Distribution of magnetic moments in a Co film along [001] calculated for the two polarizations, $P_{\downarrow}$ (left panel) and $P_{\uparrow}$ (right panel), of the PTO substrate. Results for three Co films (see Fig. 1) are shown.

Based on the geometry of the interface bond orbitals and their symmetry, one may conclude that the dominant interaction at the interface is the hybridization between Ti and Co d states, as well as between O p and Co d states. The results of our *ab initio* study indicate that this interaction induces magnetic moments on the interfacial Ti sites which are antiparallel to the magnetic moments of the neighboring Co cations. A similar theoretical analysis has been made recently for ultrathin Co and Fe films on the TiO_2-terminated $BaTiO_3$ and a detailed picture of the interactions at the interface has been reported [24]. For the $P_{\downarrow}$ state, the topmost Ti cation is relatively farther away from the first Co layer, so that the corresponding orbital hybridization is suppressed. The Co-O bond distance, however, allows for strong p-d hybridization, which leads to the marginally induced positive magnetic moments on oxygen. As the ferroelectric polarization is reversed to state $P_{\uparrow}$, the Co-O separation increases, which reduces the O moments, and more importantly, the Ti cations reach the proximity of the ferromagnetic Co layer. Due to the hybridization between the d states of these cations the negative spin polarization at the Ti site is significantly enhanced and, thereby, contributes to the MEC. The spin polarization of the interfacial Co itself is not much affected by this process.

Now we study the effect of Zr on the strength of MEC at the Co/PZT interface. The results obtained within the digital alloy model (Fig. 9) indicate the possibility of tuning the ME coupling at the interface by changing the position of the impurity. In the case of a Zr atom placed in the third atomic layer away from the interface, the total change in the interfacial magnetization is slightly enhanced in comparison with the original undoped system ($\Delta M_{\mathrm{IF}} = -0.68$ μ_B). We relate this enhancement of the interfacial MEC effect to (a) a local increase in the ionic Ti-O displacement at the interface by 0.03 Å compared to the pure PTO substrate and (b) a contraction of the Ti-Co distance, which facilitates spin-dependent charge transfer. A larger effect can be achieved by realizing the doping directly on the interface. Because of the lower degree of localization of Zr d orbitals, only a small magnetic moment is induced at the topmost Zr site for the $P_{\uparrow}$ state: -0.077 μ_B against -0.292 μ_B on Ti at the Co/PTO interface (Fig. 9). On the other hand, the MEC effect now spans three atomic layers, including the second cobalt layer IF+2. The estimated value $\Delta M_{\mathrm{IF}} = -0.58$ μ_B is again very close to that of the pure Co/PTO interface (-0.65 μ_B).

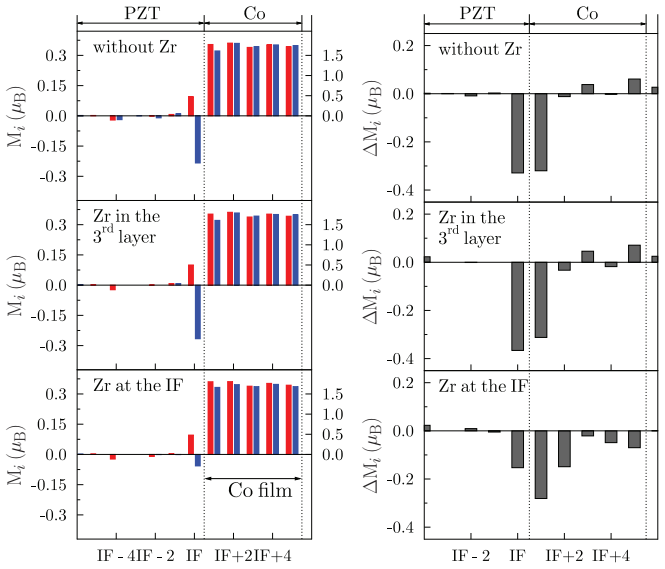

FIG. 9. (Color online) Layer-resolved magnetic moments M_i (left panel) of atomic planes near the Co/PZT (001) interface (marked by the dashed vertical line between the IF and the IF+1 ticks), compared to chemically clean Co/PTO (001). Polarizations $P_\downarrow$ ($P_\uparrow$) are shown by the left (red) and right (blue) bars in each pair. The total change in magnetization $\Delta M_i = M_i(P_\uparrow) - M_i(P_\downarrow)$ for each atomic layer in all three systems is presented in the right panel.

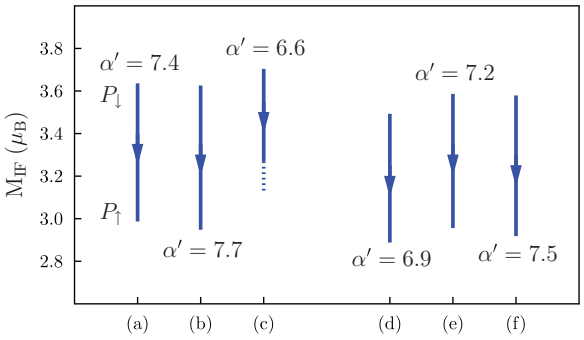

FIG. 10. (Color online) Total magnetic moment of the interfacial composition Co · BO_2 (B = Ti, Zr, Hf) in the digital alloy model—(a) Co/PTO, (b) Co/PZT with Zr in the interface layer, and (c) Co/PZT with Zr in the third layer—as well as for the larger supercells: (d) Co/PTO with a reconstructed cobalt film, (e) Co/PZT, and (f) Co/PHT with 25% Zr/Hf doping in the interface layer. Changes in magnetization under polarization reversal are shown by two points, one above the other, and the arrow connecting them (corresponds to the transition from the $P_\downarrow$ to the $P_\uparrow$ state). Estimated values of the MEC coefficient are presented in units of 10^{-10} G cm^2 V^{-1}.

This picture is supported by our simulations of the 25%-doped interface, for which we predict the induction of magnetic moments at the topmost B sites (B = Ti, Zr, Hf) and charge transfer from the metallic side similar to the mechanism described above for the pure Co/PTO system. The induced moments on the 4d (5d) cations are twice as large as those found for the digital alloy arrangement of impurities: $-0.141\ \mu_B$ and $-0.131\ \mu_B$ for Zr and Hf impurities, respectively. The total change in the interfacial magnetic moment for the 25%-doped case is confined to two or three atomic layers and lies in the range from $-0.74\ \mu_B$ to $-0.83\ \mu_B$ per surface area of one perovskite unit cell.

From the calculated interfacial magnetic moments $M_{IF}(P_\downarrow)$ and $M_{IF}(P_\uparrow)$ (Fig. 10) we obtain the value of the empirical MEC coefficient α using the expression $\alpha = \Delta M_{IF}/(AE_c)$, where the coercive field is taken to be equal to 33 kV/cm (valid for bulk PTO) and A is the surface area across the interface. Our findings demonstrate the possibility of tuning the MEC effect as well as the interface structure by introducing impurities at B sites with a larger ionic radius, such as Zr and Hf dopants. Although the induced magnetism on 4d (5d) transition-metal cations is rather marginal, enhancement of the spin polarization of the neighboring 3d cations compensates for this and the resulting MEC strength averaged over a large surface area differs by at most 7% from the undoped system. However, one could argue here that the coercive field E_c of the doped ferroelectric should be different from the bulk value of pure PTO. Indeed, according to experimental data [27] the coercive field of the PZT compound with a 50/50 composition equals 10 kV/cm, which means that for the composition studied in this work this value could be lower than we assumed, and correspondingly, the estimated MEC coefficient for the Co/PZT interface would be even higher. It would be beneficial to get more insight into the actual values of E_c for the considered structures.

The Co/PHT interface might be applicable for two reasons. First, the MEC effect on this interface exceeds that of both Co/PTO and Co/PZT structures (Fig. 10), and second, the interface itself is characterized by a moderate roughness (Fig. 5), which is beneficial for growing well-ordered nanostructures. Furthermore, the ferroelectric parameters of the PHT perovskite alloy [28] are comparable to the characteristics of the widely used PZT. This might motivate researchers to grow PHT-based multiferroic interfaces.

V. ELECTRONIC PROPERTIES

Since the MEC effect expected for the studied interface has an electronic origin, it is necessary to understand how the electronic properties of the interface depend on the ferroelectric polarization. From the site-projected DOS (Fig. 11) we see that there is an injection of states in the minority d channel in the energy range from $E_F - 2.0$ eV to E_F, leading to enhanced induced moments at B sites for the $P_\uparrow$ state, whereas the occupied d states are not significantly modified for the opposite polarization. This is accompanied by only minor changes in the electronic states for interfacial Co atoms. Spin-dependent charge transfer across the multiferroic interface involves the t_{2g} orbitals with d_{yz} (d_{xz}) symmetry, which provide the strongest overlap between the electronic states of the transition-metal cations. The Ti d_{yz} orbitals dominate in this process, since the d states of Zr (Hf) dopants are relatively delocalized and, as expected, contribute marginally to the local DOS near the Fermi level.

Based on the electronic features of the studied interface, the recently observed reversible change of sign of the TMR effect at multiferroic LSMO/PZT/Co tunnel junctions [8] might be explained within the limitations of the Julliere model [29]. The latter allows estimation of the TMR ratio from the spin

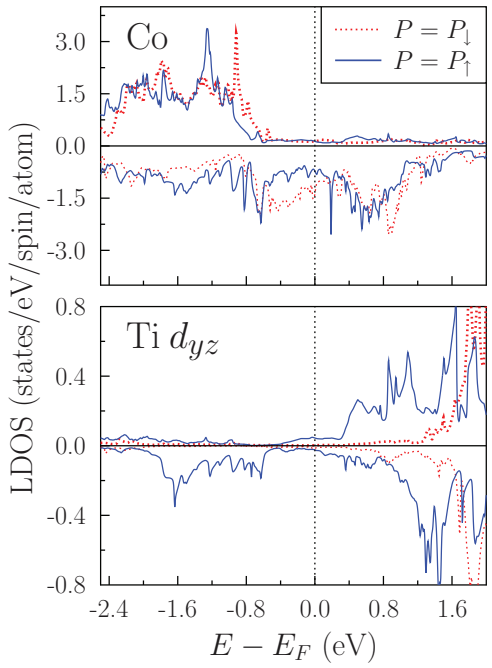

FIG. 11. (Color online) Spin-polarized DOS projected onto the Co cations (upper panel) and d_{yz} orbitals of Ti (lower panel) near the Co/PTO interface for the $P_\downarrow$ and $P_\uparrow$ polarization states [dashed (red) and solid (blue) curves, respectively].

polarizations $SP_{L,R}$ of charge carriers on the two opposite interfaces of the considered junction:

$$TMR = \frac{R_{\uparrow\downarrow} - R_{\uparrow\uparrow}}{R_{\uparrow\downarrow}} = \frac{2\,SP_L \cdot SP_R}{1 + SP_L \cdot SP_R}, \quad (1)$$

where $R_{\uparrow\uparrow}$ and $R_{\uparrow\downarrow}$ are the resistances for the parallel and antiparallel alignment of the lead magnetization, respectively. In this work, we study only the interface between Co and PZT and the sign of the corresponding spin polarization can be related to the spin imbalance $SI = n_\uparrow(E) - n_\downarrow(E)$, i.e., the difference between the spin-up and the spin-down DOS values for the chosen energy.

The fact that the TMR effect is inverse for the polarization pointing towards the Co film ($P_\uparrow$ in our setup) indicates opposite signs of the considered spin polarizations. Since the LSMO/PZT interface is not expected to be affected by the ferroelectric side due to its almost 100% half-metallic character and high magnetic stability for the chosen composition, $x = 0.33$, we conclude that the spin polarization of the other interface (Co/PZT) should be negative for the $P_\uparrow$ state to explain the observed effect. Indeed, as we see from the energy-dependent spin imbalance near the Fermi level (Fig. 12), the d_{yz} states of the interface Ti cations acquire a large negative polarization in the energy range from $E_F - 2.0$ eV to E_F. Due to the large overlap and, accordingly, the strong hybridization between Co and Ti d orbitals (also responsible for the MEC effect), we would expect the tunneling electrons at this interface to be predominantly of d character with $SP_R < 0$ for a moderate negative-bias voltage that samples the above-mentioned energy range.

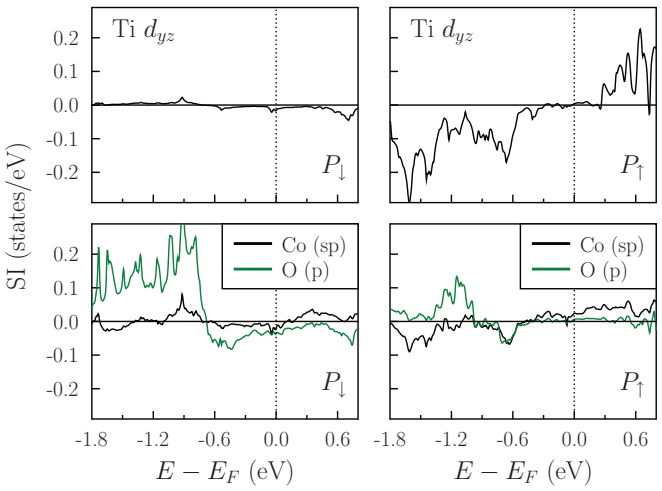

FIG. 12. (Color online) Energy-dependent spin imbalance (SI) of the hybridized sp electronic states of cobalt and p states of oxygen in the Co-O bonds and the d_{yz} states of the interface Ti cations for the $P_\downarrow$ and $P_\uparrow$ states of the Co/PTO (001) undoped interface.

Since the TMR effect has been observed to change its sign under polarization reversal [8], we assume that the considered interface becomes positively spin polarized for the $P_\downarrow$ state. In this case, the Ti cations are too distant from the first cobalt layer and the orbital hybridization is suppressed, whereas the Co-O bond is now shorter and the orbital hybridization in the Co-O pair is enhanced. Therefore, the tunneling is likely to be governed by the delocalized s and p states of these cations. We identified the largest contribution to the spin polarization, coming from the p states of oxygen, to be positive in the energy range from $E_F - 2.0$ eV to $E_F - 0.7$ eV for the $P_\downarrow$ state (Fig. 12). The combined sp states of cobalt cations contribute only marginally. Upon polarization reversal the effect of spin polarization in the ligand p states weakens considerably, which lets the Ti d_{yz} states prevail, as discussed above.

To summarize, we conclude that for the $P_\uparrow$ state the tunneling occurs mostly due to hybridized Co-Ti bonds with a negative spin polarization, leading to the inverse TMR. For the $P_\downarrow$ state, the tunneling is likely due to covalent Co-O bonds with a positive spin polarization of the ligand p states, which would explain the observation of the normal TMR effect. Our explanation of the polarization-dependent TMR ratio at LSMO/PZT/Co junctions is similar to that proposed by De Teresa *et al.* [30], also in relation to the possibly voltage-dependent character of this effect.

VI. CONCLUSIONS

In our *ab initio* study we have investigated the influence of Zr and Hf doping on the structural features and the MEC at the multiferroic interface Co/PbB_xTi$_{1-x}$O$_3$ (001) (B = Ti, Zr, Hf). Independently of the concrete interface composition, the MEC effect originates in the spin-dependent charge transfer from the metallic side into the d orbitals of the interfacial B transition-metal cations, similarly to the previously studied Fe/BaTiO$_3$ and Fe/PbTiO$_3$ systems. We have estimated the change in the interfacial magnetization in response to

polarization reversal to be of the order of 0.6–0.8 μ_B. In view of the recent experimental findings concerning LSMO/PZT/Co tunnel junctions [8] and similar LSMO/PZT heterostructures [9,10], we have discussed the relation of the MEC effect to the spin polarization of the tunneling electrons and the observed change in sign of the TMR effect induced by polarization reversal. We predict this effect to be observable over a wide energy range near the Fermi level, from $E_F - 2.0$ eV to $E_F - 0.7$ eV. It would be worthwhile performing first-principles calculations of the electronic transport to gain a better insight into the tunneling mechanism at this junction. Moreover, further studies are required to clarify the contribution of the complex LSMO/PZT interface to the observed tunneling phenomena.

Zr/Hf doping was found to affect the Co-O and Co-Ti bonding distances and to enhance locally the ferroelectric polarization. The highest interface roughness has been found for the Co/PZT system with the energetically less preferable $P_\uparrow$ state. Our simulations of the 25%-doped interface demonstrated the tendency of the cobalt layers to reconstruct in such a way as to approach the original bulk structure, which is totally different from the perfect epitaxially grown fcc structure. The formation of a nicely shaped hcp-like element in the structure of the cobalt film is observed for all studied interfaces. Rotation of this element under polarization reversal for the 25%-doped interfaces is still to be clarified. The MEC effect averaged in the in-plane direction appears to be robust with respect to weakly magnetic Zr and Hf impurities. We expect the newly considered system Co/PHT (001) with the 5*d* transition-metal cations of Hf to have an application potential comparable to that of the widely discussed Co/PZT interface. Further experimental work on the structural, electronic, and spin-dependent transport properties of these multiferroic interfaces and the corresponding tunnel junctions would contribute to the understanding of their potential for spintronics applications.

ACKNOWLEDGMENTS

We are thankful to Marin Alexe and Dietrich Hesse for fruitful discussions and insights from experimental studies. This work was supported by Sonderforschungsbereich SFB 762, Functionality of Oxide Interfaces.

[1] N. A. Spaldin and M. Fiebig, Science **309**, 391 (2005).
[2] M. Fiebig, J. Phys. D: Appl. Phys. **38**, R123 (2005).
[3] E. Tsymbal and H. Kohlstedt, Science **313**, 181 (2006).
[4] M. Bibes and A. Barthelemy, Nat. Mater. **7**, 425 (2008).
[5] V. Garcia, M. Bibes, L. Bocher, S. Valencia, F. Kronast, A. Crassous, X. Moya, S. Enouz-Vedrenne, A. Gloter, D. Imhoff *et al.*, Science **327**, 1106 (2010).
[6] S. Valencia, A. Crassous, L. Bocher, V. Garcia, X. Moya, R. O. Cherifi, C. Deranlot, K. Bouzehouane, S. Fusil, A. Zobelli *et al.*, Nat. Mater. **10**, 753 (2011).
[7] J. Hu, J. Li, and C.-W. Nan, Adv. Mater. **23**, 1062 (2011).
[8] D. Pantel, S. Goetze, D. Hesse, and M. Alexe, Nat. Mater. **11**, 289 (2012).
[9] L. Jiang, W. S. Choi, H. Jeen, S. Dong, Y. Kim, M.-G. Han, Y. Zhu, S. V. Kalinin, E. Dagotto, T. Egami *et al.*, Nano Lett. **13**, 5837 (2013).
[10] Y. W. Yin, J. D. Burton, Y.-M. Kim, A. Y. Borisevich, S. J. Pennycook, S. M. Yang, T. W. Noh, A. Gruverman, X. G. Li, E. Y. Tsymbal *et al.*, Nat. Mater. **12**, 397 (2013).
[11] G. Kresse and J. Hafner, Phys. Rev. B **49**, 14251 (1994).
[12] G. Kresse and J. Furthmüller, Phys. Rev. B **54**, 11169 (1996).
[13] J. Hafner, J. Comput. Chem. **29**, 2044 (2008).
[14] J. P. Perdew, K. Burke, and M. Ernzerhof, Phys. Rev. Lett. **77**, 3865 (1996).
[15] P. E. Blochl, Phys. Rev. B **50**, 17953 (1994).
[16] H. J. Monkhorst and J. D. Pack, Phys. Rev. B **13**, 5188 (1976).
[17] M. Fechner, S. Ostanin, and I. Mertig, Phys. Rev. B **77**, 094112 (2008).
[18] H. L. Meyerheim, F. Klimenta, A. Ernst, K. Mohseni, S. Ostanin, M. Fechner, S. Parihar, I. V. Maznichenko, I. Mertig, and J. Kirschner, Phys. Rev. Lett. **106**, 087203 (2011).
[19] H. L. Meyerheim, A. Ernst, K. Mohseni, I. V. Maznichenko, J. Henk, S. Ostanin, N. Jedrecy, F. Klimenta, J. Zegenhagen, C. Schlueter, I. Mertig, and J. Kirshner, Phys. Rev. Lett. **111**, 105501 (2013).
[20] C.-G. Duan, S. S. Jaswal, and E. Y. Tsymbal, Phys. Rev. Lett. **97**, 047201 (2006).
[21] J. D. Burton and E. Y. Tsymbal, Phys. Rev. B **80**, 174406 (2009).
[22] M. Fechner, S. Ostanin, and I. Mertig, Phys. Rev. B **80**, 094405 (2009).
[23] I. I. Oleinik, E. Y. Tsymbal, and D. G. Pettifor, Phys. Rev. B **65**, 020401 (2001).
[24] St. Borek, M. Hoffmann, I. V. Maznichenko, S. Ostanin, G. Fischer, W. Hergert, I. Mertig, A. Ernst, and A. Chasse (unpublished).
[25] T. Yamamoto, Jpn. J. Appl. Phys. **35**, 5104 (1996).
[26] M. Fechner, I. V. Maznichenko, S. Ostanin, A. Ernst, J. Henk, and I. Mertig, Phys. Status Solidi B **247**, 1600 (2010).
[27] G. H. Haertlin, Am. Ceram. Soc. Bull. **49**, 564 (1970).
[28] B. Jaffe, R. S. Roth, and S. Marzullo, J. Res. Natl. Bur. Stand. **55**, 239 (1955).
[29] M. Julliere, Phys. Lett. A **54**, 225 (1975).
[30] J. M. De Teresa, A. Barthelemy, A. Fert, J. P. Contour, F. Montaigne, and P. Seneor, Science **286**, 507 (1999).